Activity-dependent modification of inhibitory synapses in models of rhythmic neural networks

Cristina Soto-Treviño, Kurt A. Thoroughman and Eve Marder, L. F. Abbott

Volen Center and Biology Department, Brandeis University, Mail Stop 013, 415 South Street, Waltham, Massachusetts 02454-9110, USA

The first two authors contributed equally to this work

Correspondence should be addressed to K.A.T. (kurt@brandeis.edu)

The faithful production of rhythms by many neural circuits depends critically on the strengths of inhibitory synaptic connections. We propose a model in which the strengths of inhibitory synapses in a central pattern-generating circuit are subject to activity-dependent plasticity. The strength of each synapse is modified as a function of the global activity of the postsynaptic neuron and by correlated activity of the pre- and postsynaptic neurons. This allows the self-assembly, from random initial synaptic strengths, of two cells into reciprocal oscillation and three cells into a rhythmic triphasic motor pattern. This self-assembly illustrates that complex oscillatory circuits that depend on multiple inhibitory synaptic connections can be tuned via simple activity-dependent rules.

Central pattern-generating networks produce the rhythmic motor discharges that underlie many repetitive movements, such as those in locomotion, respiration and feeding[1]. Synaptic inhibition is important in the organization of virtually all central pattern generators. Alternation between functional antagonists commonly occurs as a consequence of reciprocal inhibition[2–4], and in some cases, reciprocal inhibition provides the actual mechanism by which rhythmic motor patterns are produced[5–11]. In many central pattern-generating networks, neuronal firing depends on rebound from inhibition[12–15], and modulation of the strength of inhibitory synapses can produce dramatic changes in the motor patterns produced[16]. The critical role of inhibitory synapses in central pattern generating networks makes it crucial to understand how their strengths are regulated, both during development and throughout adult life.

Much effort has been spent on understanding how neuronal activity regulates the strength of excitatory synapses. The regulation of synaptic inhibition has received much less attention, despite the fact that all neuronal networks contain numerous inhibitory connections, and circuit function requires that both inhibitory and excitatory pathways be appropriately regulated. Some inhibitory synapses display long-term modification of strength[17–23]. In the cerebellum, the amount of Ca^{2+} that enters the postsynaptic neuron during a post-inhibitory rebound depolarization seems to determine whether long-term potentiation or long-term depression of inhibitory synapses occurs[23]. Postsynaptic increases in Ca^{2+} concentration evoked by metabotropic receptors are thought to be crucial for the induction of long-term potentiation of inhibitory synapses in developing visual cortex[22]. Thus, changes in postsynaptic Ca^{2+} concentrations seem to be part of the intracellular signaling pathways needed to control inhibitory synaptic strength.

In this study, we explore theoretically a set of activity-dependent rules that tune synaptic strengths in models of small rhythmic networks. We analyze a simple two-cell reciprocally inhibitory circuit, and then a three-cell model of the pyloric network of the stomatogastric ganglion (STG) of decapod crustaceans. This circuit is ideal for our study because it generates a triphasic motor pattern[24] in which the individual neurons must fire in a particular sequence. We demonstrate that network models can self-assemble to generate specific alternating or triphasic motor patterns using two simple activity-dependent rules of synaptic modification, one that depends on the activity level of the postsynaptic neuron and one that depends on both pre- and postsynaptic activity.

Results

Activity-dependent regulation in a two-cell circuit

Because reciprocal inhibition is at the core of many central pattern-generating networks (including the STG[1]), our first goal was to design a synaptic modification rule that would allow two neurons to self-assemble into a circuit in which the two neurons fired in alternation. In this first analysis, we study three cases: two tonically depolarized neurons, two oscillators and one of each. The parameters of these model neurons were chosen so that the tonically depolarized neuron mimicked properties of the lateral pyloric (LP) cell, and the oscillator mimicked the lumped properties of the anterior burster (AB) and pyloric dilator (PD) cells in the STG. We therefore call the tonically depolarized cell LP and the oscillator AB/PD. Synaptic transmission in the STG is both spike-mediated and graded, but it is thought that most neurotransmitter release is associated with graded transmission that follows from the slow changes in membrane potential seen in Fig. 3a[25,26]. We therefore model only the slow changes in membrane potential underlying rhythmic behavior using the nonspiking Morris–Lecar equations[27] (Methods).

We investigated the behavior of the two-LP cell circuit over a range of equal and unequal synaptic strengths (Fig. 1a–e). This is in contrast to previous work in which two-cell reciprocally inhibitory circuits were studied under conditions in which the two synapses were identical[28,29]. When uncoupled, these neurons were

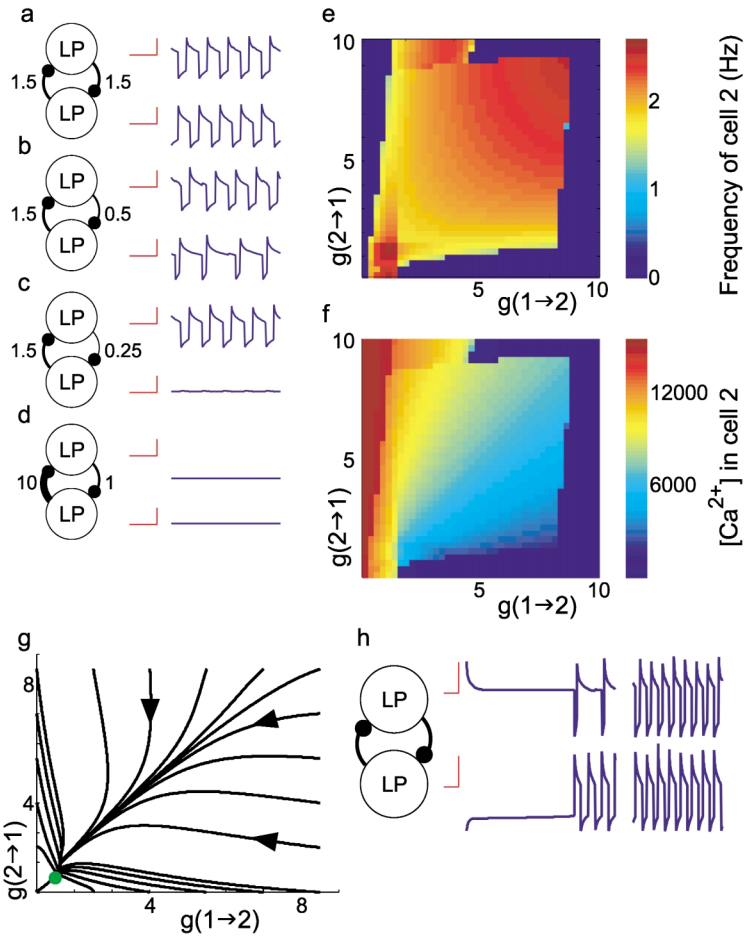

Fig. 1. Behavior at fixed coupling and activity-dependent modification of LP-LP two-cell circuit. (**a–d**) Voltages of the two cells at four different strengths of synaptic coupling. Scale bars, 50 mV and 250 ms. Numbers next to synaptic connections indicate the strength of each synapse. (**e**) Frequency of cell 2 of the LP-LP circuit over a range of the two synaptic strengths. The color scale displays frequency in Hz; 0 Hz (dark blue) indicates that cell 2 is not oscillating. (**f**) Calcium concentration (in $\mu C/cm^2$; see Methods) in cell 2 over the same range of synaptic strengths. (**g**, **h**) Modification of synapses via global rule (Equation 3). (**g**) Trajectories of synaptic strengths during modification, from many initial synaptic strengths. The fixed point to which all trajectories lead is indicated with a green dot. Arrowheads, direction of modification. (**h**) Voltage traces during modification from a single initial condition. Scale bars, 50 mV and 500 ms. In all figures, synaptic conductances *g* are expressed in mS/cm^2.

constantly depolarized (Fig. 3b); in a spiking model, they would fire tonically. At steady state, the oscillation frequency of each neuron depends nonlinearly on the strengths of both synapses. Within one range of synaptic conductances, the neurons form an oscillator, with each cell depolarizing in alternation (as in Fig. 1a). At other strengths of inhibitory synaptic connections, the two cells produce varying oscillatory or non-oscillatory behaviors. If the strength of the synapse inhibiting one cell is reduced from the value necessary for reciprocal oscillation, both cells oscillate but with unequal frequencies (Fig. 1b). Further reduction of the strength of this synapse causes the postsynaptic cell to stop alternating between hyperpolarization and depolarization, although it produces small oscillations above 0 mV (Fig. 1c). Pairing a weak inhibitory synapse to one cell with a strong inhibitory synapse to the other causes the two cells to clamp, respectively, at depolarized and hyperpolarized voltages (Fig. 1d).

We sought a simple sensor that, despite the complex relationship between synaptic strength and oscillation frequency, could drive the tuning of the synapses to produce a desired oscillatory behavior. Intracellular calcium has been suggested as an appropriate sensor of average voltage activity for the tuning of intrinsic conductances[30–32]. Therefore, postsynaptic intracellular calcium concentration could be the simple sensor that controls the modification of inhibitory synaptic strength. To determine whether intracellular calcium concentration would be appropriate to drive tuning in our model inhibitory circuit, we integrated the calcium current to generate an intracellular calcium concentration (see Methods). As one inhibitory synaptic conductance increases while the other is held fixed, the intracellular calcium concentration monotonically decreases in the cell postsynaptic to the synapse increasing in strength (Fig. 1f).

The consistent gradient of postsynaptic calcium across synaptic strengths suggested that a synaptic modification rule that modifies a synapse in proportion to the difference between the actual calcium concentration and a target value ($[Ca]_{tgt}$) could control synaptic strengths to produce, for example, symmetric rhythmicity. Implementing this rule (Methods, Equation 3) in the two-LP cell circuit, with the time constant of the regulation process slow relative to the cycle period, did indeed drive circuits with many initial synaptic strengths into a single set of strengths (Fig. 1g), determined by the value of $[Ca]_{tgt}$, at which the two cells oscillated symmetrically. Voltage traces for one particular set of initial synaptic strengths (Fig. 1h) show that between no oscillation and 1:1 alternation, the network passes through synaptic strengths that produce patterns other than 1:1 alternation.

The rhythmic frequency of cells in circuits consisting of two intrinsic bursters (AB/PD-AB/PD, Fig. 2a) or one of each cell type (AB/PD-LP, Fig. 2c) also depends nonlinearly on the strength of both synapses. Because the AB/PD cells intrinsically oscillate, cells oscillate in the AB/PD-AB/PD circuit over a wide range of synaptic strengths, but both cells oscillate at the same frequency over a relatively small band of synaptic strengths. The LP cell in the AB/PD-LP circuits, on the other hand, oscillates in 1:1 entrainment over a wide range of frequencies sandwiched between regions of no oscillation and 2:1 entrainment with the AB/PD. Despite differences between these circuits and the LP-LP pairs, tuning of each inhibitory synapse via postsynaptic calcium concentration successfully drives all initial pairs of synaptic strengths into a single final pair of strengths (Fig. 2a and c) at which the cells oscillate in 1:1 entrainment (Fig. 2b and d).

The pyloric network model

We now move from two-cell circuits to a three-cell circuit built to generate the pyloric rhythm of the STG, as illustrated in the simultaneous intracellular recordings in Fig. 3a. STG neurons show considerable postinhibitory rebound[12,33], which depends

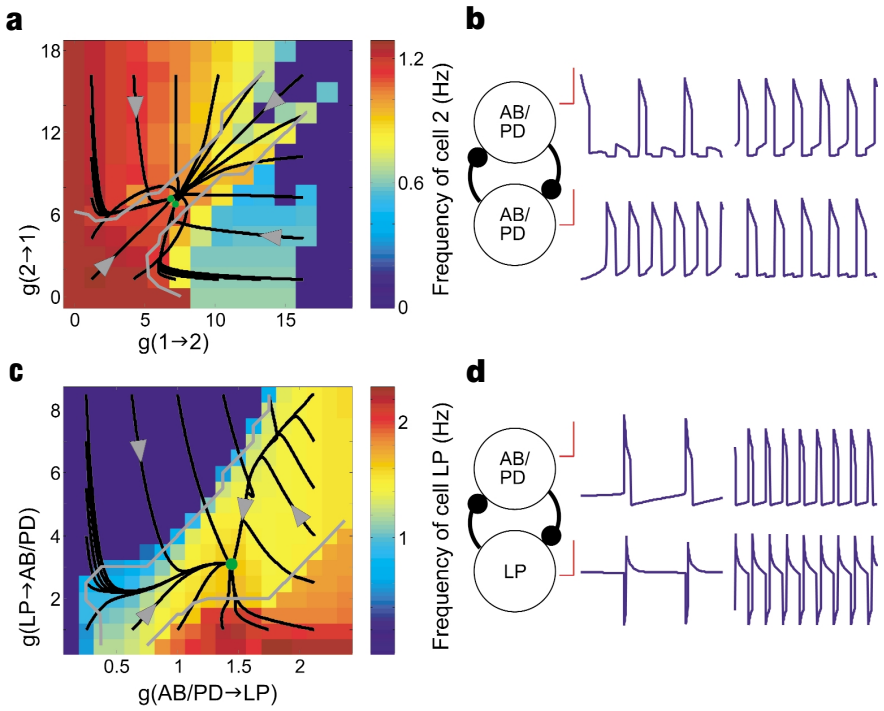

Fig. 2. Behavior at fixed coupling and activity-dependent modification of AB/PD-AB/PD and AB/PD-LP two-cell circuits. Color plots, frequency at fixed coupling of the second cell (the second AB/PD in **a**, the LP in **c**), as a function of the strength of both synapses. Superimposed on the frequency color plots are trajectories of synaptic strength during modification, from many initial synaptic strengths (as in **Fig. 1g**). Fixed points are indicated with green dots. The AB/PD-AB/PD circuits in (**a**) converge on the synaptic strength pair (6.82, 7.19); which synapse converges on which value depends on initial strengths (hence there are two dots). Also superimposed, silver lines that demark the central region in which the two cells in the circuit fire in 1:1 entrainment (as in **Fig. 1a** in the LP-LP case). Remaining plots, voltage traces during modification from single initial conditions in AB/PD-AB/PD (**b**) and AB/PD-LP (**d**) circuits.

on the strength and duration of the inhibitory postsynaptic potential[12–14,16]. The anterior burster (AB) neuron and the pyloric dilator (PD) neurons, which depolarize synchronously, are electrically coupled and together form the pacemaker for the pyloric rhythm. We therefore model these as a single 'pacemaker' neuron called AB/PD (Fig. 3b). The intrinsic membrane properties of each type of STG neuron are different, and therefore somewhat different parameters (Table 1) are used for the three model neurons. Like the LP cell, the isolated pyloric (PY) neuron is tonically depolarized and would fire tonically if we modeled action potentials. The model LP neuron recovers from inhibition more rapidly than the model PY neuron (Fig. 3b), as is true of their biological counterparts[12,34].

When the model neurons are connected with the synaptic architecture of the pyloric network and appropriate synaptic strengths (Fig. 3c, right), an alternating triphasic pattern is generated that mimics the biological pyloric rhythm (Fig. 3a). The LP neuron is inhibited by AB/PD, but escapes from this inhibition to fire and inhibit AB/PD. The PY neurons then depolarize, escaping from LP's inhibition and simultaneously inhibiting LP. Our goal is to find synaptic tuning rules that allow the circuit to self-assemble into the triphasic pattern in which neurons are active in the order AB/PD, then LP, then PY.

The connectivity diagram in Fig. 3c shows the five synaptic connections, all of which are subject to activity-dependent modification. In this network, the LP and PY neurons are inhibited by two different neurons, but the pacemaker neuron receives feedback only from the LP neuron.

Synaptic regulation in the pyloric network

In the pyloric network, the model LP and PY neurons receive inhibition from two different presynaptic neurons that fire at different times in the cycle (Fig. 3). A single global regulation rule, as used in the two-cell circuit, can only jointly strengthen or weaken all synapses onto a given postsynaptic neuron; it cannot change the ratios between their synaptic strengths. We nevertheless first asked how well a global rule alone, such as in the two-cell networks, would work in the three-cell case. These simulations ($n = 121$) started from random initial synaptic strengths, in the range between 80% greater than and 80% less than the canonical strengths used to generate the standard triphasic rhythm (Fig. 3c). A substantial number (45%) of these initial synaptic strengths produced the desired triphasic rhythm

Table 1. Intrinsic conductances, gating variables and time constants of model neurons.

	AB/PD	LP	PY
g_L	2	5	5
g_K	20	15	12
g_{Ca}	8	20	19
$m_\infty(V)$	$\frac{1}{2}(1+\tanh(\frac{V+20}{25}))$	$\frac{1}{2}(1+\tanh(\frac{V+10}{20}))$	$\frac{1}{2}(1+\tanh(\frac{V+4}{25}))$
$\tau_\infty(V)$	$(0.0008\cosh(\frac{V+5}{40}))^{-1}$	$(0.008\cosh(\frac{V}{30}))^{-1}$	$(0.0025\cosh(\frac{V}{30}))^{-1}$
$n_\infty(V)$	$\frac{1}{2}(1+\tanh(\frac{V+20}{8}))$	$\frac{1}{2}(1+\tanh(\frac{V+10}{5}))$	$\frac{1}{2}(1+\tanh(\frac{V}{15}))$
$s^{j\to i}(V)$	$(1+\exp(\frac{-V-50}{15}))^{-1}$	$(1+\exp(\frac{-V-58}{10}))^{-1}$	$(1+\exp(\frac{-V-56}{10}))^{-1}$

For s, the presynaptic cell determined parameters; the column label is therefore cell j in the notation $s^{j\to i}(V)$. Voltages are in mV, the time constant τ is in ms, and conductances g_x are in mS/cm^2.

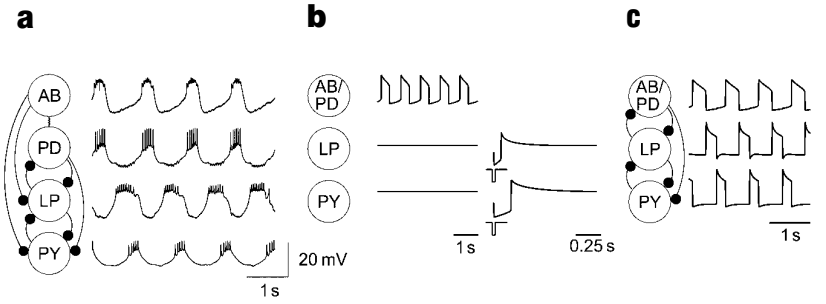

Fig. 3. Biological and model STG neurons. (**a**) Wiring diagram and typical voltage traces of four biological STG cells producing a pyloric rhythm. The AB and PD cells are electrically coupled; all other synapses are inhibitory. (**b**) Model cells in isolation. A single cell represents the coupled AB/PD pair and oscillates when isolated. The LP and PY cells are tonically depolarized when isolated. In response to a hyperpolarizing pulse, the PY cell remains hyperpolarized longer and decays more slowly to the steady state than the LP cell. (**c**) The target triphasic pattern of activity produced when the three model cells are coupled with appropriate fixed inhibitory synaptic strengths.

before any synaptic modification. Another 46% of the initial conditions were driven by the global rule into synaptic strengths that produced the desired rhythmicity. The remaining 9% of the three-cell circuits, however, did not produce the triphasic rhythm either initially or after tuning with the global rule alone.

Certain initial synaptic strengths do not lead to the desired triphasic rhythm via the mechanism of the global rule because the linked weakening or strengthening of both synapses onto a neuron could not produce synaptic strengths appropriate for the triphasic rhythm. Because the global rule preserves the ratio of synaptic strengths coming into each postsynaptic cell, any synaptic tuning that does not differentially regulate individual synapses cannot generate the desired triphasic rhythm out of these initial conditions. For example, when the PY to LP synapse is five times the strength of the AB/PD to LP synapse, and the AB/PD to PY synapse is five times as strong as the LP to PY synapse, the global rule can produce only three behaviors, all undesired: one or more cells not oscillating, all cells oscillating in unequal entrainment, or all cells oscillating in equal entrainment but with up phases in the undesired order (AB/PD, followed by PY, and then LP).

In an attempt to adapt all initial synaptic strengths to the desired values, we added a term to the adaptation rule that could differentially regulate individual synapses (Methods, Equation 4). This synapse-specific term depends on both the presynaptic voltage and the postsynaptic calcium current (Fig. 4a). The dependence on presynaptic voltage is sigmoidal, such that the strength of a particular synapse can change only when the presynaptic cell is depolarized. Whereas the global rule depends on the difference between actual and target calcium concentration, the synapse-specific rule depends on the difference between actual and target calcium currents. The synapse-specific term therefore features greater temporal precision to better reflect the contribution of each individual active synapse. The use of the calcium current in this rule corresponds to a dependence on the concentration near the cell membrane, which is proportional to the calcium current. In contrast, the global rule depends on the bulk intracellular calcium concentration. As with the global rule, the time constant of the regulation process is slow relative to the cycle period of oscillations in voltages and calcium currents.

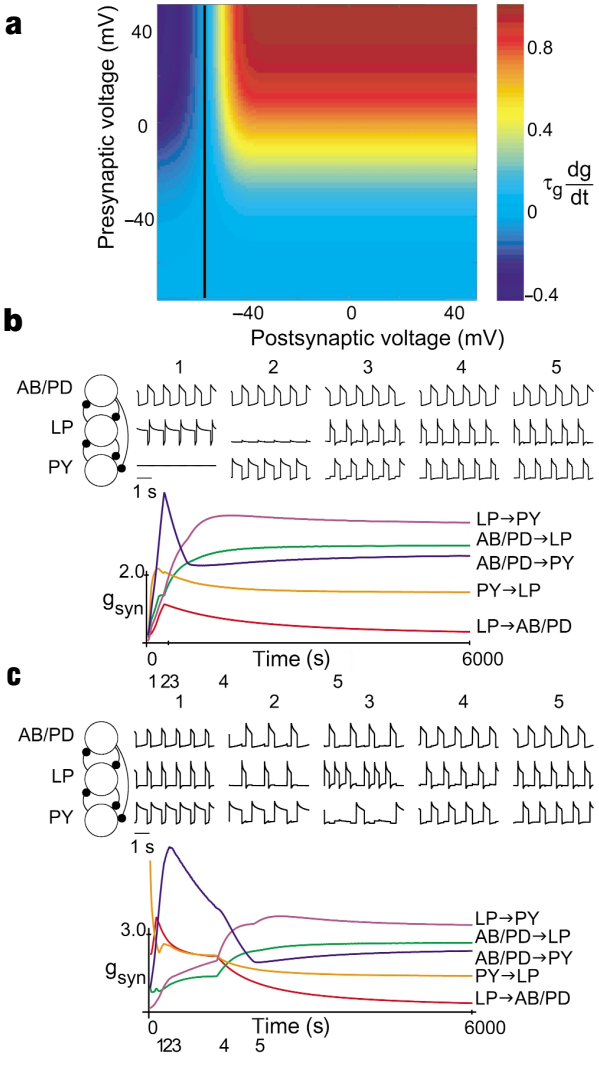

Fig. 4. Synapse-specific term; development of triphasic rhythm in model three-cell network. (**a**) Dependency of the synapse-specific term (in Equation 4) on pre- and postsynaptic voltage. The rule depends on calcium current, which is a function of voltage; this plot shows the direct dependence on voltage. Positive values indicated on the color bar lead to strengthening of a synapse. (**b**, **c**) Voltage and synaptic strength traces as the synapses of the model circuit are modified by activity. The five sets of voltage traces in (**b**) and (**c**) correspond to snapshots of activity taken at the times indicated by numbers underneath the synaptic strength changes. In (**b**), the AB/PD and LP cells are initially oscillating, but the PY cell is tonically depolarized. In (**c**), two cells are initially oscillating in synchrony. In both cases, the synaptic modification rule (Equation 4) develops synaptic strengths that produce a triphasic rhythm.

Fig. 5. Convergence of synaptic strengths in the three-cell circuit from many initial values to a unique set of strengths via activity-dependent tuning (Equation 4). Because the circuit has five (not six) synapses, one synaptic strength (LP→AB/PD) is repeated in the top and bottom plots. Across plots, lines of the same color represent the same simulation run. Asymptotic values of synaptic strengths are shown with a green dot.

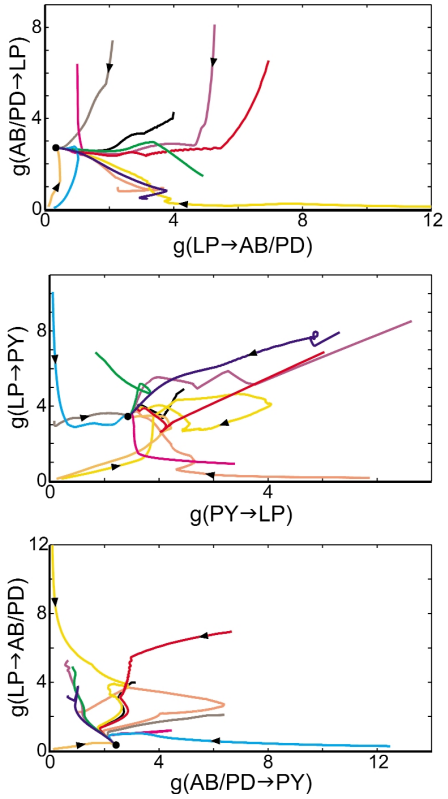

To determine whether these activity-dependent rules allow the network to generate the desired triphasic pattern from different initial conditions, we carried out multiple runs of the model in which the synaptic conductances were randomly assigned initial values. Each run was long enough for the synapses to come to equilibrium. In all of these runs, all five synaptic strengths converged onto a single fixed point, at which the circuit oscillated in the target triphasic pattern.

In one such run (Fig. 4b), the strengths of all of the synapses were initially very low. Under these conditions, the AB/PD neuron oscillated, the LP neuron fired in phase with the AB/PD, and the PY neuron was locked in a depolarized state (Fig. 4b, panel 1). Over time, the synaptic modification rule caused each of the synapses to increase in strength. At the time shown in panel 2, the LP neuron became completely inactive, because the strength of the two synapses to it became too large. The PY neuron at this time fired in alternation with the AB/PD neuron. By the time of panel 3, a triphasic pattern was established, and the remaining changes in synaptic strength allowed the triphasic rhythm to settle into its equilibrium. Another run (Fig. 4c) began with very different initial synaptic strengths. Early in the run, the AB/PD and LP neurons fired in synchrony. As the run continued, the network produced a variety of different output patterns, until again it converged onto the target triphasic motor pattern. Across many runs of the model, trajectories taken by synaptic strengths (Fig. 5) were quite different, as were the specific dynamics of the evolution of the motor pattern. In all of the runs, however, synaptic strengths converged to a final equilibrium value at which the network produced the target triphasic rhythm.

Discussion

This model suggests that relatively simple rules can tune the strengths of the inhibitory synapses in a central pattern-generating network. The trajectories of the motor patterns and their associated synaptic strengths show considerable irregularity as the networks converge toward the final, desired motor pattern. The strengths of individual synapses may increase, decrease, then increase again, and the motor patterns may go through a regime in which they seem less regular than the initial output. STG motor patterns are considerably more irregular early in development than in the adult[35]. Embryonic central pattern-generating networks, including those of the STG, are active before they are needed behaviorally[4,35–37]. This early activity could provide 'tuning signals' for the developing networks.

The final output of any circuit depends on the interaction of each neuron's intrinsic membrane properties and the strengths of the synapses between the neurons. In previous models, in which synaptic strengths were held constant, stable triphasic rhythms evolved from activity-dependent self-tuning of intrinsic membrane currents[38]. In the work reported here, we held the intrinsic properties of the neurons constant, but focused on the regulation of synaptic strengths. During development and adult life, intrinsic

Table 2. Values of parameters in the synaptic tuning rule used in two-cell circuits (Equation 3).

	AB/PD in AB/PD-AB/PD	AB/PD in AB/PD-LP	LP in LP-LP	LP in AB/PD-LP
$[Ca]_{tgt}$ ($\mu C/cm^2$)	2250	1750	9000	11500

Table 3. Values of parameters in the synaptic tuning rule used in three-cell circuits (Equation 4). For σ, the presynaptic cell determined parameters.

	AB/PD	LP	PY
$I_{Ca,tgt}$ (mA/cm^2)	31	29	30
$[Ca]_{tgt}$ ($\mu C/cm^2$)	2500	4500	4500
$\sigma(V)$	$(1+\exp(\frac{-V-10}{15}))^{-1}$	$(1+\exp(\frac{-V-10}{10}))^{-1}$	$(1+\exp(\frac{-V-10}{10}))^{-1}$

membrane properties and synaptic strengths must presumably be coordinately tuned, which will be addressed in future models.

The two rules of synaptic plasticity suggested here are not based specifically on experimental work on plasticity of synapses in the STG, but they are inspired by recent biological findings. The global activity-dependent rule depends on Ca^{2+} entry during postinhibitory rebound and captures the spirit of data from the cerebellum[23]. The global rule is sufficient to drive two-cell circuits to reciprocal oscillation, and in three-cell circuits is sufficient to drive 90% of randomly initialized synaptic strengths into the triphasic rhythm. If, during development, the initial synaptic strengths had approximately appropriate ratios, the global rule alone could create and maintain appropriate rhythmic output. If not, the addition of a synapse-specific rule would allow any initial synaptic strengths to be regulated to generate a triphasic rhythm. Such a rule could be biologically instantiated by the activation of a metabotropic receptor on the postsynaptic neuron[22] or by retrograde signaling. The model predicts that clamping a postsynaptic STG neuron at a depolarized or hyperpolarized voltage would induce an increase or decrease in inhibitory synaptic strength, respectively, and that plasticity of a synapse between two oscillating cells would depend on the relative timing between the pre- and postsynaptic depolarized phases. The model further predicts that plasticity would be blocked by preventing calcium influx or by injecting a calcium chelator in the postsynaptic cell.

Here we suggest a simple and biologically plausible mechanism for inhibitory synaptic tuning, but do not claim that this solution is unique. In particular, the time constants used in simulations were chosen so that, during rhythmic oscillations, calcium concentrations were reasonably constant (requiring τ_{Ca} to be longer than the circuit's oscillation period) and synaptic modifications were not susceptible to small calcium transients ($\tau_g > \tau_{Ca}$). Other combinations of time constants may drive circuits to desired rhythmicity, but with more time-varying synaptic strengths.

In central pattern-generating networks, the existence of a rhythm allows for the identification of target values for the calcium concentrations and currents. These targets in turn drive synaptic strengths to values for which the network produces canonical behavior. In the example shown here, the well-defined pyloric rhythm makes the determination of appropriate synaptic strengths relatively easy. In other systems, the determination of when inhibition is correctly tuned may be more difficult. We speculate that rhythms might provide signals for the calibration of inhibitory synaptic strengths in other neural networks, such as cortical circuits, in which excitatory and inhibitory synapses coexist but rhythm production is not a primary function of the network.

Methods

Model neurons. Each neuron was modeled by the following equations.

$$
\begin{aligned}
C\frac{dV^i}{dt} &= -I_L^i - I_K^i - I_{Ca}^i - I_{syn}^i \\
I_L^i &= g_L^i (V^i - E_L) \\
I_K^i &= g_K^i n^i (V^i - E_K) \\
\tau_\infty^i (V^i)\frac{dn^i}{dt} &= n_\infty^i (V^i) - n^i \\
I_{Ca}^i &= g_{Ca}^i m_\infty^i (V^i)(V^i - E_{Ca}) \\
I_{syn}^i &= [g^{j\to i} s^{j\to i}(V^j) + g^{k\to i} s^{k\to i}(V^k)](V^i - E_{syn})
\end{aligned}
\qquad (1)
$$

Here, C denotes capacitance, I the transmembrane current, V the transmembrane potential, E the reversal potential, and g conductance; the subscripts L, K, Ca and syn denote leak, potassium, calcium, and synaptic; n is the activation gating variable of I_K; m_∞ and s are the activation gating variables of I_{Ca} and I_{syn}; and superscripts are indices of neurons, with $j\to i$ indicating the synaptic connection from cell j to cell i. Cell capacitance and reversal potentials for all cell types were $C = 1\ \mu F/cm^2$, $E_L = -50$ mV, $E_K = -80$ mV, $E_{Ca} = 100$ mV, and $E_{syn} = -80$ mV. Cell types were differentiated by their intrinsic conductances and by parameters in their voltage-dependent gating variables and time constants (Table 1).

Synaptic tuning. The intracellular calcium concentration was integrated from the calcium current as specified by the following equation.

$$\frac{d[\mathrm{Ca}]}{dt} = -I_{\mathrm{Ca}} - \frac{[\mathrm{Ca}]}{\tau_{Ca}} \qquad (2)$$

Although ionic concentrations are typically reported in mol/l, here we express [Ca] in units of ionic charge per unit surface area ($\mu C/cm^2$; $1\ \mu C = 1\ mA \times 1\ ms$). In both two- and three-cell circuits, varying the rate of calcium dynamics by a factor of 100 did not affect the final values of synaptic strengths. Tuning of each synapse in the two-cell circuits was proportional to the difference between instantaneous and target calcium concentrations inside the postsynaptic cell:

$$\tau_g \frac{dg^{j\to i}}{dt} = \frac{([\mathrm{Ca}]^i - [\mathrm{Ca}]^i_{\mathrm{tgt}})g^{j\to i}}{[\mathrm{Ca}]^i_{\mathrm{tgt}}} \qquad (3)$$

where $\tau_g = 35$ s. The frequency of asymptotic oscillation of the two-cell circuit depended on the particular values of $[\mathrm{Ca}]_{\mathrm{tgt}}$; values used to produce the simulations in Figs. 1 and 2 were chosen by surveying the range of synaptic strengths and setting $[\mathrm{Ca}]_{\mathrm{tgt}}$ to the typical average intracellular calcium concentration during symmetric oscillation (Table 2).

In the three-cell circuit, modification of each synapse depended on the presynaptic potential and on both the postsynaptic calcium current and intracellular calcium concentration.

$$\tau_g \frac{dg^{j\to i}}{dt} = g^{j\to i}\left(\sigma^j(V^i)\tanh\left(-\frac{I_{\mathrm{Ca}}^i - I_{\mathrm{Ca,tgt}}^i}{50}\right) + \frac{[\mathrm{Ca}]^i - [\mathrm{Ca}]^i_{\mathrm{tgt}}}{3}\right) \qquad (4)$$

where $\tau_g = 35$ s and $\sigma(V)$ is a sigmoidal function of postsynaptic voltage, with parameters that depend on the identity of the presynaptic cell (Table 3). The overall dependence of the synapse-specific term

$$\left(\sigma^j(V^i)\tanh\left(-\frac{I_{\mathrm{Ca}}^i - I_{\mathrm{Ca,tgt}}^i}{50}\right)\right)$$

on pre- and postsynaptic voltage is shown in Fig. 4a. Targets of calcium concentration and calcium current in each cell (Table 3) were determined by surveying the range of synaptic strengths and identifying, in those circuits that produced the desired triphasic rhythm, typical average calcium concentrations and typical calcium currents coincident with presynaptic depolarization. Asymptotic modification of synapses was characterized as reaching a fixed point if all synaptic strengths remained unchanged up to at least three decimal places.

Acknowledgements

This research was supported by MH 46742, NS 07292 and the Sloan and Keck Foundations.

Received 11 October 2000; Accepted 22 January 2001

1. Marder, E. & Calabrese, R. L. Principles of rhythmic motor pattern generation. *Physiol. Rev.* 76, 687–717 (1996).
2. Brown, T. G. On the nature of the fundamental activity of the nervous centres; together with an analysis of the conditioning of rhythmic activity in

progression, and a theory of the evolution of function in the nervous system. *J. Physiol. (Lond.)* 48, 18–46 (1914).
3. Grillner, S., Parker, D. & el Manira, A. Vertebrate locomotion—a lamprey perspective. *Ann. NY Acad. Sci.* 860, 1–18 (1998).
4. Sillar, K. T., Reith, C. A. & McDearmid, J. R. in *Neuronal Mechanisms for Generating Locomotor Activity* Vol. 860 (eds. Kiehn, O., Harris-Warrick, R. M., Jordan, L. M., Hultborn, H. & Kudo, N.) 318–332 (New York Academy of Sciences, New York, 1998).
5. Arbas, E. A. & Calabrese, R. L. Slow oscillations of membrane potential in interneurons that control heartbeat in the medicinal leech. *J. Neurosci.* 7, 3953–3960 (1987).
6. Angstadt, J. D. & Calabrese, R. L. Calcium currents and graded synaptic transmission between heart interneurons of the leech. *J. Neurosci.* 11, 746–759 (1991).
7. Nadim, F., Olsen, Ø. H., De Schutter, E. & Calabrese, R. L. Modeling the leech heartbeat elemental oscillator. I. Interactions of intrinsic and synaptic currents. *J. Comput. Neurosci.* 2, 215–235 (1995).
8. Olsen, Ø. H., Nadim, F. & Calabrese, R. L. Modeling the leech heartbeat elemental oscillator. II. Exploring the parameter space. *J. Comput. Neurosci.* 2, 237–257 (1995).
9. Olsen, Ø. H. & Calabrese, R. L. Activation of intrinsic and synaptic currents in leech heart interneurons by realistic waveforms. *J. Neurosci.* 16, 4958–4970 (1996).
10. Satterlie, R. A. Reciprocal inhibition and postinhibitory rebound produce reverberation in a locomotor pattern generator. *Science* 229, 402–404 (1985).
11. Friesen, W. O. Reciprocal inhibition: a mechanism underlying oscillatory animal movements. *Neurosci. Biobehav.* 18, 547–553 (1994).
12. Hartline, D. K. & Gassie, D. V. Jr. Pattern generation in the lobster (Panulirus) stomatogastric ganglion. I. Pyloric neuron kinetics and synaptic interactions. *Biol. Cybern.* 33, 209–222 (1979).
13. Harris-Warrick, R. M., Coniglio, L. M., Barazangi, N., Guckenheimer, J. & Gueron, S. Dopamine modulation of transient potassium current evokes phase shifts in a central pattern generator network. *J. Neurosci.* 15, 342–358 (1995).
14. Harris-Warrick, R. M., Coniglio, L. M., Levini, R. M., Gueron, S. & Guckenheimer, J. Dopamine modulation of two subthreshold currents produces phase shifts in activity of an identified motoneuron. *J. Neurophysiol.* 74, 1404–1420 (1995).
15. Miller, J. P. & Selverston, A. I. Mechanisms underlying pattern generation in lobster stomatogastric ganglion as determined by selective inactivation of identified neurons. IV. Network properties of pyloric system. *J. Neurophysiol.* 48, 1416–1432 (1982).
16. Eisen, J. S. & Marder, E. A mechanism for production of phase shifts in a pattern generator. *J. Neurophysiol.* 51, 1375–1393 (1984).
17. Marty, A. & Llano, I. Modulation of inhibitory synapses in the mammalian brain. *Curr. Opin. Neurobiol.* 5, 335–341 (1995).
18. Korn, H., Oda, Y. & Faber, D. S. Long-term potentiation of inhibitory circuits and synapses in the central nervous system. *Proc. Natl. Acad. Sci. USA* 89, 440–443 (1992).
19. Oda, Y., Charpier, S., Murayama, Y., Suma, C. & Korn, H. Long-term potentiation of glycinergic inhibitory synaptic transmission. *J. Neurophysiol.* 74, 1056–1074 (1995).
20. Oda, Y., Kawasaki, K., Morita, M., Korn, H. & Matsui, H. Inhibitory long-term potentiation underlies auditory conditioning of goldfish escape behaviour. *Nature* 394, 182–185 (1998).
21. Komatsu, Y. & Iwakiri, M. Long-term modification of inhibitory synaptic transmission in developing visual cortex. *Neuroreport* 4, 907–910 (1993).
22. Komatsu, Y. $GABA_B$ receptors, monoamine receptors, and postsynaptic inositol trisphosphate-induced Ca^{2+} release are involved in the induction of long-term potentiation at visual cortical inhibitory synapses. *J. Neurosci.* 16, 6342–6352 (1996).
23. Aizenman, C. D., Manis, P. B. & Linden, D. J. Polarity of long-term synaptic gain change is related to postsynaptic spike firing at a cerebellar inhibitory synapse. *Neuron* 21, 827–835 (1998).
24. Harris-Warrick, R. M., Marder, E., Selverston, A. I. & Moulins, M. (eds.) *Dynamic Biological Networks: The Stomatogastric Nervous System* (MIT Press, Cambridge, Massachusetts, 1992).
25. Graubard, K., Raper, J. A. & Hartline, D. K. Graded synaptic transmission between spiking neurons. *Proc. Natl. Acad. Sci. USA* 77, 3733–3735 (1980).
26. Graubard, K., Raper, J. A. & Hartline, D. K. Graded synaptic transmission between identified spiking neurons. *J. Neurophysiol.* 50, 508–521 (1983).
27. Morris, C. & Lecar, H. Voltage oscillations in the barnacle giant muscle fiber. *Biophys. J.* 35, 193–213 (1981).
28. Skinner, F. K., Kopell, N. & Marder, E. Mechanisms for oscillation and frequency control in reciprocal inhibitory model neural networks. *J. Comput. Neurosci.* 1, 69–87 (1994).
29. Wang, X.-J. & Rinzel, J. Alternating and synchronous rhythms in reciprocally inhibitory model neurons. *Neural Comp.* 4, 84–97 (1992).
30. LeMasson, G., Marder, E. & Abbott, L. F. Activity-dependent regulation of conductances in model neurons. *Science* 259, 1915–1917 (1993).
31. Liu, Z., Golowasch, J., Marder, E. & Abbott, L. F. A model neuron with activity-dependent conductances regulated by multiple calcium sensors. *J. Neurosci.* 18, 2309–2320 (1998).
32. Siegel, M., Marder, E. & Abbott, L. F. Activity-dependent current distributions in model neurons. *Proc. Natl. Acad. Sci. USA* 91, 11308–11312 (1994).
33. Hartline, D. K., Russell, D. F., Raper, J. A. & Graubard, K. Special cellular and synaptic mechanisms in motor pattern generation. *Comp. Biochem. Physiol.* 91C, 115–131 (1988).
34. Tierney, A. J. & Harris-Warrick, R. M. Physiological role of the transient potassium current in the pyloric circuit of the lobster stomatogastric ganglion. *J. Neurophysiol.* 67, 599–609 (1992).
35. Richards, K. S., Miller, W. L. & Marder, E. Maturation of the rhythmic activity produced by the stomatogastric ganglion of the lobster, *Homarus americanus*. *J. Neurophysiol.* 82, 2006–2009 (1999).
36. Casasnovas, B. & Meyrand, P. Functional differentiation of adult neural circuits from a single embryonic network. *J. Neurosci.* 15, 5703–5718 (1995).
37. O'Donovan, M. J. The origin of spontaneous activity in developing networks of the vertebrate nervous system. *Curr. Opin. Neurobiol.* 9, 94–104 (1999).
38. Golowasch, J., Casey, M., Abbott, L. F. & Marder, E. Network stability from activity-dependent regulation of neuronal conductances. *Neural Comp.* 11, 1079–1096 (1999).